Biological Control 179 (2023) 105176

Contents lists available at ScienceDirect

Biological Control

journal homepage: www.elsevier.com/locate/ybcon

Tree pathogens *Armillaria solidipes* influence the biocontrol activity of *Bacillus velezensis* BY6

Ping Zhang [a,b,*], Hao Xin [b], Theo van der Lee [a]

[a] *Biointeractions and Plant Health (Wageningen University & Research), Wageningen 6700 AA, Netherlands*
[b] *Heilongjiang Provincial Key Laboratory of Forest Sustainable Management and Environmental Microbial Engineering (Northeast Forestry University), Harbin 150040, China*

HIGHLIGHTS

- Pathogen *A. solidipes* inhibited the late biological control effect of BY6.
- Pathogen *A. solidipes* disrupted the BY6 cell wall and cell membrane.
- Pathogen *A. solidipes* restricted BY6 intracellular nutrient utilization.
- Pathogen *A. solidipes* downregulated the expression of BY6 spore and biofilm formation genes.

GRAPHICAL ABSTRACT

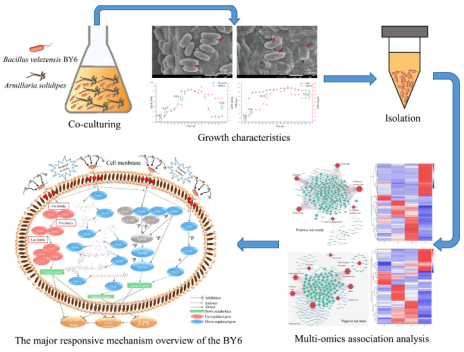

ARTICLE INFO

Keywords:
Bacillus velezensis
Armillaria solidipes
Transcriptomic
Biological control
Metabolomic

ABSTRACT

This is the first-time work to integrate transcriptome and metabolome sequencing data, providing a comprehensive knowledge of how the pathogen *Armillaria solidipes* affects the spore development, biofilm creation, and antifungal activity of *Bacillus velezensis* BY6. The dynamic growth of BY6 indicated that *A. solidipes* had a significant growth-inhibiting effect on BY6. Using scanning electron microscopy (SEM), it was discovered that the cell wall and cell membrane was compromised, resulting in the leakage of intracellular components. On the basis of gene and metabolite network analysis, several genes and metabolites are predominantly involved in the " Phosphotransferase system (PTS)", "Two-component system", and "Ubiquinone and other terpenoid-quinone biosynthesis" pathway. The mechanism by which *A. solidipes* inhibits the biological control ability of BY6 is influenced by numerous factors, including cell membrane damage (Folding, disintegration, disappearance), nutrient limitation (Pyruvic acid, Menadione concentration down-regulated), and spore and biofilm formation inhibition (*Spo0 A*, *Spo0 B* and *Kin B* ~ *D* genes down-regulated). We conclude that interference of *A. solidipes* with the growth and development of BY6 results in a decrease in BY6 biocontrol levels. This result contributes to a complete and thorough understanding of the mechanism by which *A. solidipes* inhibits BY6's biocontrol ability and identifies additional potential molecular targets. To further genetically modify the BY6 strains for tackle the problem of drug resistance.

* Corresponding author at: Biointeractions and Plant Health (Wageningen University & Research), Wageningen 6700 AA, Netherlands.
E-mail address: ping.zhang@wur.nl (P. Zhang).

https://doi.org/10.1016/j.biocontrol.2023.105176
Received 25 October 2022; Received in revised form 7 January 2023; Accepted 25 January 2023
Available online 2 February 2023

1. Introduction

Armillaria root rot (ARR) is a devastating disease on many different trees and shrubs including pine (*Pinus*), Popular (*Populus*) and Apple (*Malus domestica*), and disease management in natural forests and production sites is extremely challenging. For decades, implemented chemical control strategies have relied on a limited number of available fungicides (carbendazim) with only a few distinct modes (affects cell division) of action (Casamali and Chavez, 2017; Kedves et al., 2021). The fungicides currently applied in forests and orchards have a low efficacy and are insufficient to control diseases such as ARR. Alternative fungicides with a higher efficacy are restricted because of their negative impact on the environment (Teklu et al., 2022). New measures to control ARR are therefore urgently needed and options for biological control have been explored (Kedves et al., 2021). Endophytes of the genus *Bacillus* species are considered an attractive alternative to conventional pesticides in plant disease management (Eljounaidi et al., 2016). In addition to the ability to promote plant growth (Alotaibi et al., 2022), various species of *Bacillus* spp. have been shown to suppress disease by different modes of action, including (i) induction of systemic resistance (ISR) in plants (Kloepper et al., 2004; Stoll et al., 2021), (ii) production of antimicrobial compounds (Ghendov-Mosanu et al., 2022), and (iii) competition for space (Jautzus et al., 2022) or (iv) nutrients (Dimopoulou et al., 2021). The later three modes of action indicate a direct interaction between the biocontrol agent and the pathogen. Although multiple mechanisms are likely to operate synergistically and in parallel to obtain the beneficial protective effects of *Bacillus* spp., production of antimicrobial compounds appears to be one of the most critical factors contributing to their biocontrol efficiency (Ongena and Jacques, 2008).

Bacillus velezensis is the most investigated species in the genus, with 5–8% of its genome devoted to the production of antimicrobial compounds, such as hydrolases enzymes, volatile compounds, bacteriocins, polyketides and lipopeptides (LPs) (Chun et al., 2019). These antimicrobial compounds have important effects on phytopathogenic microorganisms. We have previously selected biocontrol strains of popular tree endophytes belonging to *Bacillus* based on their ability to produce spores. We selected *Bacillus velezensis* BY6 and have shown its efficacy in biocontrol and plant growth promotion (Zhang et al., 2022b). We observed a clear and strong inhibition zone when co-culturing *Armillaria solidipes* and BY6, but also noticed that *A. solidipes* showed re-growth upon prolonged culture on the edge of the colony, this indicates that the battle between these two micro-organisms continues. As are expected to be present in the same ecological niche (the xylem in the popular trunk), and likely would interact directly, we studied this direct interaction at a molecular level. In the past, such studies on the interaction were often limited to the initial screening and assessment of antifungal effects of *Bacillus* spp (Zhang et al., 2022a). However, the interaction is more complex and reciprocally in the interaction with plant pathogenic bacteria and fungi, *Bacillus* spp. are likely to be confronted with antimicrobial compounds produced by these pathogens. *Bacillus* spp. counter act such adverse conditions by producing resistant spores and releasing antimicrobial compounds and extracellular polymers (ExoPolySaccharides, EPS) (Radhakrishnan et al., 2017). The EPS are of general importance, as it can promote the formation of *Bacillus* biofilms and protect them to survive in harsh environments (Jha et al., 2022). Here we specifically study the effect of *A. solidipes* on BY6 were we considered several aspects in an integrated, time-dependent study, (i) biofilm formation, (ii) morphogenesis, (iii) transcription and (iv) metabolics in BY6 cells.

Biofilms act as a protective barrier to prevent pathogens from attempting to enter plants. The secretion of secondary metabolites with antimicrobial activity can directly counteract pathogen attacks. Biofilms can be composed of single species but also of heterogeneous populations of motile, matrix-producing, and spore-forming cells (Kilic and Cihan, 2020). They exhibit adhesion to each other's surfaces through a complex matrix medium. This matrix medium contains a variety of EPS, spore concentration (*OD600*), and environmental DNA (eDNA), which are crucial for the production capacity of *Bacillus* spp. (Vlamakis et al., 2013; Kilic and Cihan, 2020). *B. velezensis* QST713 was previously shown to form biofilms on inert surfaces and inhibit the growth of *Trichoderma aggressivum f. europaeum* to control the mushroom *Agaricus bisporus* green mold disease (Pandin et al., 2019). Previous work characterized and quantified *B. velezensis* secondary metabolites for their antagonistic activity against *Xylella fastidiosa* pathogens of almond, citrus, grapevine, and olives (Chun et al., 2019; Alotaibi et al., 2022), and correlated secondary metabolites secreted by these strains with biocontrol capabilities (Saravanakumar et al., 2019). In addition studies have shown that the biofilm of *B. velezensis* is regulated by signals from the pathogen and can have a major impact on the bacteria's biocontrol ability (Yao and Allen, 2007; Kulimushi et al., 2017). Previously, we have observed that the anti-fungal activity of BY6 was reduced after longer incubation times (>72 h) therefore we conducted an in-depth study of this loss of activity. We speculate that this phenomenon is related to BY6 metabolic inhibition and inducer repression. A large number of previous report have found that "Phosphotransferase system (PTS)", "Two-component system", and "Ubiquinone and other terpenoid-quinone biosynthesis" pathway control nitrogen metabolism, regulate iron, potassium Homeostasis, regulation of virulence in some pathogens, it also mediates the stress response under stress conditions such as nutritional stress and physical and chemical factor stimulation(Reizer et al., 1999; Kang et al., 2021; Mandinia et al., 2017; Xu et al., 2019). Through in-depth research on the mechanism of BY6 drug resistance, key targets are identified, new strategies are adopted to reduce the drug resistance of bacteria, and the bactericidal activity of ARR pathogens is greatly improved, so as to promote the development of new drugs and provide guidance.

We performed statistical analysis with on RNA-seq data and metabolomic analysis. The results were subsequently mapped by gene ontology (GO) and Kyoto encyclopedia of genes and genomes (KEGG); This allowed us to identify the three main pathways involved in this interaction.

2. Materials and method

2.1. Bacterial strains

BY6 strain was isolated from healthy *Populus* xylem and stored in the collection of Heilongjiang Provincial key laboratory of forest sustainable management and environmental microbial engineering. Its complete genome information has been stored in DDBJ/ENA/GenBank, the accession number CP051011-CP051012 (Zhang et al., 2021).

2.2. Effects of co-culturing with A. solidipes on BY6 growth

To verify the effect of the pathogen *A. solidipes* (registered in the Northeast Forestry University Center for Type Culture Collection; A2001) on the growth of BY6, we monitored the growth and development of BY6 during co-cultivation. BY6 was first activated from the storage at 4 °C by inoculation on PDA plates and sub-cultured for 2 generations. Subsequently, BY6 was transferred by a picker into a 500 mL Erlenmeyer flask containing 200 mL PD liquid medium and cultured overnight at 25 °C and 120 rpm to a mid-log phase (*OD600*) of about 1.0 x10^6 CFU/mL. The obtained fermentation broth was concentrated by low-speed centrifugation at 25 °C and 3000 rpm/min, rinsed three times with sterile water to remove the residual culture broth, and resuspended in an equal volume of PD liquid medium to prepare a bacterial suspension. A total of 0.5 g of *A. solidipes* fresh rhizomorph tissue was added to 30 mL of BY6 fermentation broth in a conical flask. The same volume of PD broth was added to the control group. The samples were cultured in conical flasks for 72 h at 25 °C and 120 rpm/min, during which the *OD600* values of the bacterial suspensions were measured every 4 h. To avoid depletion of carbohydrates during the experiment glucose was added (277.8 mmol/L) after 12 h, 24 h and 48 h (after samples were

taken). Six biological replicates were set up for each treatment.

Determination of the eDNA content released by free cells: The collected bacterial culture was subjected to protein precipitation, 900 μL of the culture was taken into a sterile 1.5 mL centrifuge tube and centrifuged at 6800 g for 4 min. A total of 500 μL of supernatant was transferred to a new centrifuge tube, mixed with 50 μL of phenol–-chloroform-isoamyl alcohol (ratio = 25:24:1), and centrifuged at 12,000 rpm/min for 10 min. Subsequently, 100 μL of the supernatant was transferred into a 96-well black microtiter plate and the amount of DNA was determined using PicoGreen® according to the instructions of the manufacturer (Invitrogen™, ThermoFisher, Waltham, USA) and the fluorescence intensity was measured with a fluorescence microplate reader (PerkinElmer, ThermoFisher, Waltham, USA) (excitation wavelength 485 nm/emission wavelength 535 nm, 0.1 s).

EPS was determined by the phenol-sulfuric acid method (Zhang et al., 2008). The steps are as follows: put the BY6 culture obtained in the above experiment into a 50 mL centrifuge tube, and centrifuge at 5000 g at 4 °C for 15 min to remove the bacteria. Collect the supernatant, mix the collected supernatant with 3 times the volume of absolute ethanol, and let stand at 0 °C–4°C for 48 h. The supernatant was discarded, and the remaining mixture was centrifuged continuously, and the collected precipitate was the EPS crude extract. EPS crude extracts were treated with DNase I (100 μg mL^{-1}) at 37 °C for 1 h, and then treated with proteinase K (100 μg mL^{-1}) at 60 °C for 1 h, The absorbance value of the obtained EPS sample was measured at a wavelength of 490 nm, and the EPS content was calculated.

Scanning electron microscopy (SEM) was used to observe the BY6 cell morphology and the *A. solidipes* rhizomorph surface to understand the interaction and competitive ability. After 0 h and 72 h of co-cultivation, the rhizomorph was imaged. The rhizomorph surface sections were fixed with 1 % glutaraldehyde as described (Zhu et al., 2021), and ethanol was used for step-wise dehydration. The inferior rhizomorph surface inoculum morphology was observed using an SEM (JSM-7500F, Tōkyō, Japan).

2.3. Total RNA extraction and sequencing library preparation

Total RNA of the cell was extracted from each treatment group. RNA isolation was performed by RNA prep pure Bacteria Kit (Tiangen, Beijing, China) following the manufacturer's instructions. RNA purity was measured using a NanoPhotometer® 2000 spectrophotometer (Implen, CA, USA). RNA integrity was assessed using the RNA Nano 6000 Assay Kit of the Agilent Bioanalyzer 2100 system (Agilent Technologies, CA, USA). A total amount of 3 μg RNA per sample was used as input material for the RNA sample preparations. cDNA libraries were produced using a NEBNext® Ultra™ RNA Library Prep Kit (NEB, USA) for Illumina, following the manufacturer's instructions. PCR products were purified (AMPure XP system, USA), and library quality was assessed using an Agilent Bioanalyzer 2100 system (Agilent Technologies, USA). Finally, the index-coded samples were clustering on a cBot Cluster Generation System by TruSeq PE Cluster Kit v3-cBot-HS (Illumina) according to the manufacturer's instructions. After cluster generation, the library preparations were sequenced on an Illumina Nova seq platform, and 150 bp paired-end reads were generated. For each time point three biological replicates were available.

2.4. Transcriptomics bioinformatic analysis

To ensure the quality of data in subsequent analysis, FASTX-Toolkit (V 0.0.13, https://hannonlab.cshl.edu/fastx_toolkit/index.html) was used to remove sequences containing adapters, N-containing and low-quality (q-value $\leq$ 30 higher than 30%) to obtain clean reads. Bowtie 2 version 2.1.0 software was used for species with higher gene density such as bacteria, to map clean reads to the previously assembled BY6 genome (Langmead and Salzberg, 2012). To eliminate the influence of sequencing quality difference and gene length on the calculated gene expression, the Fragments Per Kilobase of exon model per Million mapped fragments (FPKM) method was used to calculate the gene expression level. Before analyzing the differential gene expression, the MA-plot-based with the Random Sampling model (MARS) model in the differentially expressed gene (DEG) seq R package was used to normalize the obtained sequences numerically, and genes were selected that were in at least two groups of samples (Anders and Huber, 2012). Genes were selected as differentially expressed when the expression difference fold (Fold change) > 2 and the false discovery rate (FDR, q-value) < 0.001. Finally, GO performed functional classification statistics on genes with substantial differences in the anchored reference BY6 genome (DDBJ/NCBI/EMBL databases accept number CP051011-CP051012. To explore the functions of differentially expressed genes, Bio-tools: kobas (https://bio.tools/kobas) software was used to test DEG pathways in the KEGG statistically.

2.5. Metabolome extraction and HPLC-MS analysis

Based on the observed changes of BY6, we selected four-time points of 0 h (unexposed), 6 h (exposed), 24 h (exposed), and 72 h (exposed) for BY6 metabolome sequencing. From each sample, 50 mL of fermentation broth was centrifuged at 12,000 rpm at 4 °C for 1 min, after removing the supernatant, the bacterial samples were freeze-dried for 72 h, and homogenized using a tissue grinder. A mixture of lyophilized bacterial tissue (30 mg) and internal standard (20 μL) was spiked into a clean centrifuge tube. Methanol (750 μL) and ammonium acetate (5 mM, 750 μL) were added and samples were vortexed for 1 min at room temperature. After sonication for 20 min at room temperature, samples were centrifuged (17,000 g/min for 10 min). The supernatant (>1 mL) was transferred to a 1.5 mL tube, subsequently, 50 μL of the supernatant was transferred to a new centrifuge tube. After drying the supernatant and injecting the standard solution with 50 μL, the samples were vortexed 30 s, left at 4 °C for 10 min, then centrifuged at 13,000 rpm for 10 min, and subsequently we transferred the supernatant to an HPLC vial as described previously (Bertini et al., 2014).

Non-targeted metabolomic analysis of bacterial tissues was performed on HPLC-MS (Model: Thermo Vanquish HPLC and Thermo QE-HF-X mass spectrometer) using a Thermo Hyperil Gold column (Particle size 1.8 μm, 100 × 2.1 mm). Mobile phase A was 0.1% formic acid aqueous solution, mobile phase B was methanol, the flow rate was 300 μL, the column temperature was 10 °C, and the running time was 16 min. The mass resolution at m/z 200 is 40,000, and the mass range is 100–1500 m/z. To improve data accuracy and precision, we use a combination of positive and negative ion modes. In the positive and negative ion modes, 2 μL was injected, respectively, the spray voltage was 3200 V, kept the probe temperature was at 350 °C, and the capillary temperature was 320 °C.

2.6. Metabolome bioinformatic analysis

We employed one-way analysis (T-test and one-way ANOVA) to calculate statistical significance and changes in metabolites between control and treatment groups at different time points. Since the multivariate method considers all variables, we use the multivariate method for comprehensive data analysis using unsupervised techniques. Principal Component Analysis (PCA) and Partial Least Squares Discrimination Analysis (PLS-DA) were used to compare the metabolite differences between the treatment group and the control group, The Variable Importance in the Projection (VIP) value was used as the first principal component of the PLS-DA model, combined with the p-value of T-test to find differentially expressed metabolites, the threshold was set to VIP $>$ 2.0, and the fold difference FC > 2.0 or FC < 0.5 and p-value < 0.05. Hierarchical clustering analysis was performed on the obtained differential metabolites in each group, and the relative quantitative values of differential metabolites were transformed into Z values ($z = (x - \mu) / \sigma$: x is a specific score, μ is the mean, σ is the standard deviation) and used for

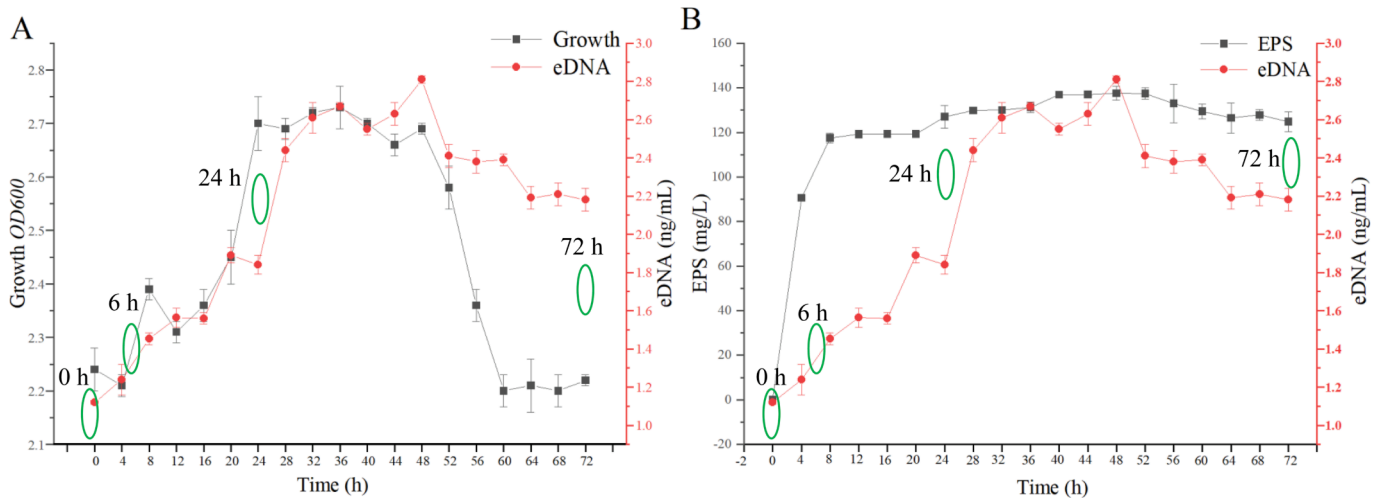

Fig. 1. *A. solidipes* affect BY6 biofilm formation and growth in liquid plate culture. BY6 growth (*OD600* nm) (A) and EPS concentration (ng/mL) (B) in planktonic cultures of BY6. Green ovals represent transcriptomic and metabolomic sampling time points. (For interpretation of the references to colour in this figure legend, the reader is referred to the web version of this article.)

clustering. Pathway analysis of the identified important metabolites was performed by the *Bacillus* spp. Pathway library and the KEGG (https://www.genome.jp/KEGG/pathway.html) was used to find the most important metabolites in *Bacillus* spp. library.

2.7. Functional analysis of integrated metabolomic and transcriptomic data

On transcriptomic and HPLC-MS metabolomic data, we constructed a Co-expression network. The genes with significant differences in transcriptome analysis and metabolites with significant differences in metabolomics analysis were correlated based on Pearson's (FDR < 0.05) correlation coefficient to measure the degree of association between DEGs and DMs. The top 50 differential metabolites (Sorted by *P* value from small to large) were selected as were the top 100 differential expressed genes (sorted by *P* value from small to large). All the differential genes and differential metabolites were mapped to the KEGG pathway database, and the common pathway information was retrieved. Subsequently, the main pathways in which differential metabolites and genes are involved were determined. Analysis of shared KEGG pathway results based on metabolic transcriptional associations was performed as follows: each pair considers the up-regulated and down-regulated metabolites in a shared pathway as well as the up-regulated and down-regulated genes in a shared pathway; subsequently, the differential genes of each comparison pair are combined linked by the differential metabolism.

The differential genes and metabolites sharing the same pathway were constructed by Cytoscape software v3.9.1 to build a network interaction map (Otasek et al., 2019). Web analytics parameter was treating the network as undirected visualize, size degree (low value to small size), clustering coefficient (low valve to bright), Map edge size to between, Map edge collar to (low values to bright). In the network, the relative importance of each gene is determined by degree of centrality. the degree centrality is defined as the number of links to a node. In addition, to study some characteristics of the network, the group attribute layout mode is used to simplify the complex network.

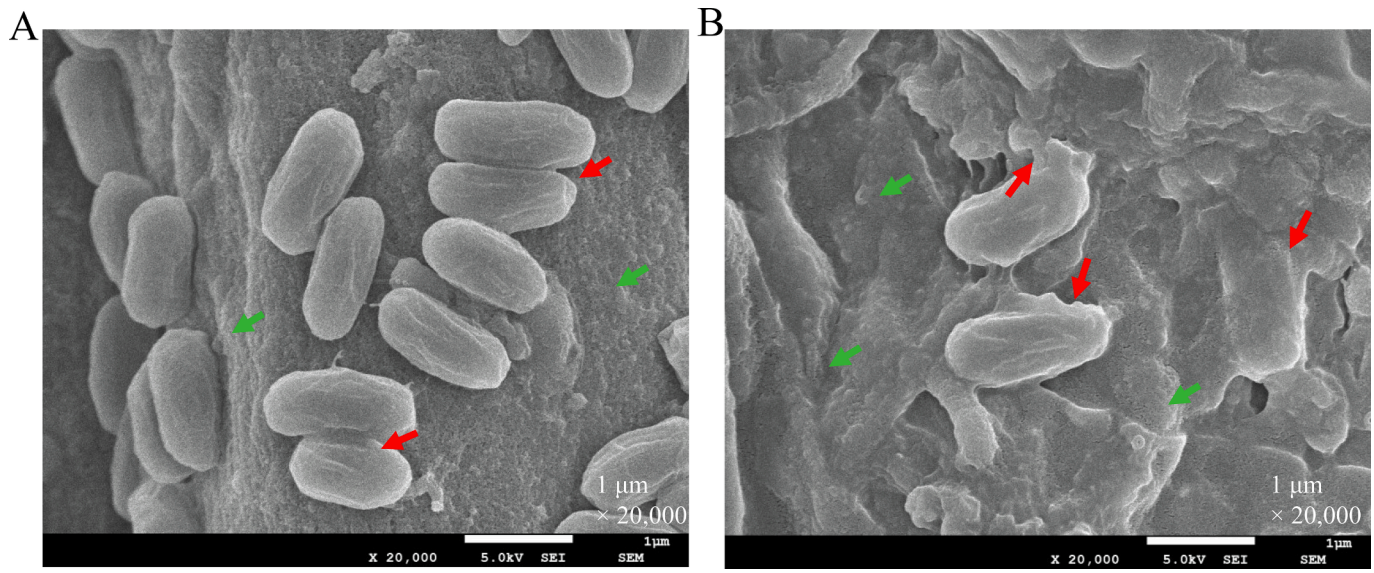

Fig. 2. Cell morphology observation of BY6 under *A. solidipes* stress Scanning electron microscope (SEM). (A) Control (0 h), (B) Treatment (72 h). BY6 cell and *A. solidipes* rhizomorph morphological characteristics by red and green arrows, respectively. (For interpretation of the references to colour in this figure legend, the reader is referred to the web version of this article.)

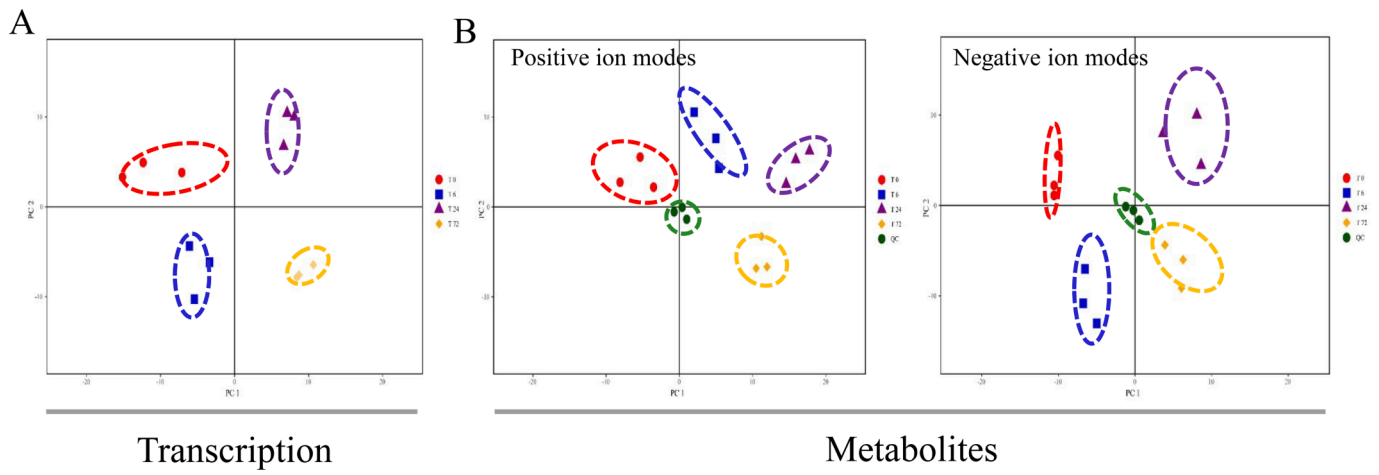

Fig. 3. PCA statistical analysis of BY6 transcription (A) and metabolites (B). T0, T6, T24 and T72 indicate that *A. solidipes* infected BY6 for 0 h vs 6 h, 0 h vs 24 h and 0 h vs 72 h, respectively.

2.8. Validation of RNA sequencing

To validate the results of RNA sequence, 24 DEGs (17 down-regulated and 7 up-regulated) were subjected to quantitative real-time PCR (qRT-PCR). Primers were designed using Primer3Plus software (https://www.primer3plus.com/) **(Table S1)**, and the primers were synthesized (Sangon Biotech, Shanghai, China), and the purified mode was ULTRAPAGE. Total RNA was extracted from each sample using RNA prep pure Bacteria Kit (Tiangen, Beijing, China). RNA quantified test using a NanoDrop 2000 spectrophotometer (Thermo Fisher Scientific, USA), and integrity was assessed by electrophoresis on agarose gels. qRT-PCR was performed using Master Mix and TB Green qPCR Kit (TaKaRa, Dalian, China) with the following thermal cycling conditions: 95 °C for 30 s, followed by 40 cycles of 95 °C for 5 s and 59 °C for 30 s. For each treatment three biologically replicated were used.

3. Results

3.1. Effects of co-culturing with A. solidipes on BY6 growth

Over a period of 72 h we monitored the secretion of eDNA, EPS and *OD600* by BY6. During co-cultivation, the concentration of BY6 cells, as determined by the eDNA and *OD600*, decreased from 0 h to 4 h, subsequently increased rapidly from 8 h to 36 h, and then stabilized and decreased after 40 h **(**Fig. 1**A)**. In contrast, the EPS concentration rises rapidly from 0 h to 8 h, stabilizes from 8 h to 52 h, and then begins to decline until 72 h **(**Fig. 1**B)**. All these key factors indicated that the growth of BY6, the production of extracellular polysaccharide and the release of eDNA were strongly affected during the co-cultivation with *A. solidipes*. As observed by SEM we identified that the BY6 cells at 72 h (treatment group) and 0 h (control group) had significant changes in morphology **(**Fig. 2**).** The BY6 cells in the control group were intact, with a smooth surface, no obvious depressions and holes, and aggregated tightly with each other in a biofilm **(**Fig. 2**A)**. In contrast, cells treated with *A. solidipes* were severely deformed, twisted and scattered, with many wrinkles, dents and breaks in the cell wall **(**Fig. 2**B)** Clearly, *A. solidipes* had a strong negative impact on the viability and growth potential of BY6. The impact of co-cultivation with *A. solidipes* was studied at a molecular level on a selection of key time points by applying a multi-omics approach.

3.2. Sequencing and de novo assembly of the transcriptome

High-throughput RNA sequencing produced 30.48 Gb of clean sequence data **(Table S2)**. The GC content of all samples exceeded 45.92%. The Q30 base percentage was at least 93.02% and Q20 base percentage was at least 97.5%. These sequencing data were considered suitable for further analysis. PCA score maps show that the clear separation of transcriptome between the different timepoints (T0, T6, T24 and T72) with a good correlation within the biological replicates of a similar time point **(**Fig. 3**)**.

Differentially Expressed Genes (DEGs) were identified by comparing RNA sequence data from the T6, T24 and T72 treatment with that of the T0 control group ($|\log^2$ (fold change) $| > 1$, FDR < 0.05). Comparing the T0 vs T6 groups of DEGs **(Fig S1)**, there were 1850 DEGs in total (919 up-regulated and 931 down-regulated DEGs). Comparing the T0 vs T24 groups of DEGs, there were 1878 DEGs in total (DEGs for 942 up-regulated and 936 down-regulated). Comparing the T0 vs T72 groups of DEGs, there were 2256 DEGs in total (1156 up-regulated and 1100 down-regulated DEGs).

3.3. Functional annotation of DEGs

Functional categories of DEGs were annotated by GO enrichment analysis, DEGs were divided into three classes including biological process of all samples, molecular function and cellular component based on the GO enrichment analysis. As listed in **Table S3**, comparing the T0 vs T6 groups, 2373 DEGs were identified using GO functional analysis (1876 up-regulated and 1870 down-regulated DEGs). In the biological process category, "Localization" (312 up-regulated and 661 down-regulated DEGs) was the most common term, followed by "Establishment of localization" (305 up-regulated and 637 down-regulated DEGs) and "Transport" (304 up-regulated and 632 down-regulated DEGs). In the cellular component category, the most abundant term was "Membrane" (379 up-regulated and 846 down-regulated DEGs). In the Molecular function category, the most common term was "Transporter activity" (185 up-regulated and 382 down-regulated DEGs)". Comparing the T0 vs T24 2350 DEGs were identified using GO functional analysis (1855 up-regulated and 1767 down-regulated DEGs). In the biological process category, "Symbiont process" (30 up-regulated and 54 down-regulated DEGs) was the most common term. In the cellular component category, the most abundant term was "Membrane" (364 up-regulated and 846 down-regulated DEGs). In the Molecular function category, most significant changes were found in "Transferase activity, transferring acyl groups other than amino-acyl groups" (61 up-regulated and 113 down-regulated DEGs). Comparing the T0 vs T72 groups of GO, 2563 DEGs were identified using GO functional analysis (1973 up-regulated and 2035 down-regulated DEGs). In the biological process category, "Transmembrane transport" (140 up-regulated and 230 down-regulated DEGs) was the most common term. The most common term in

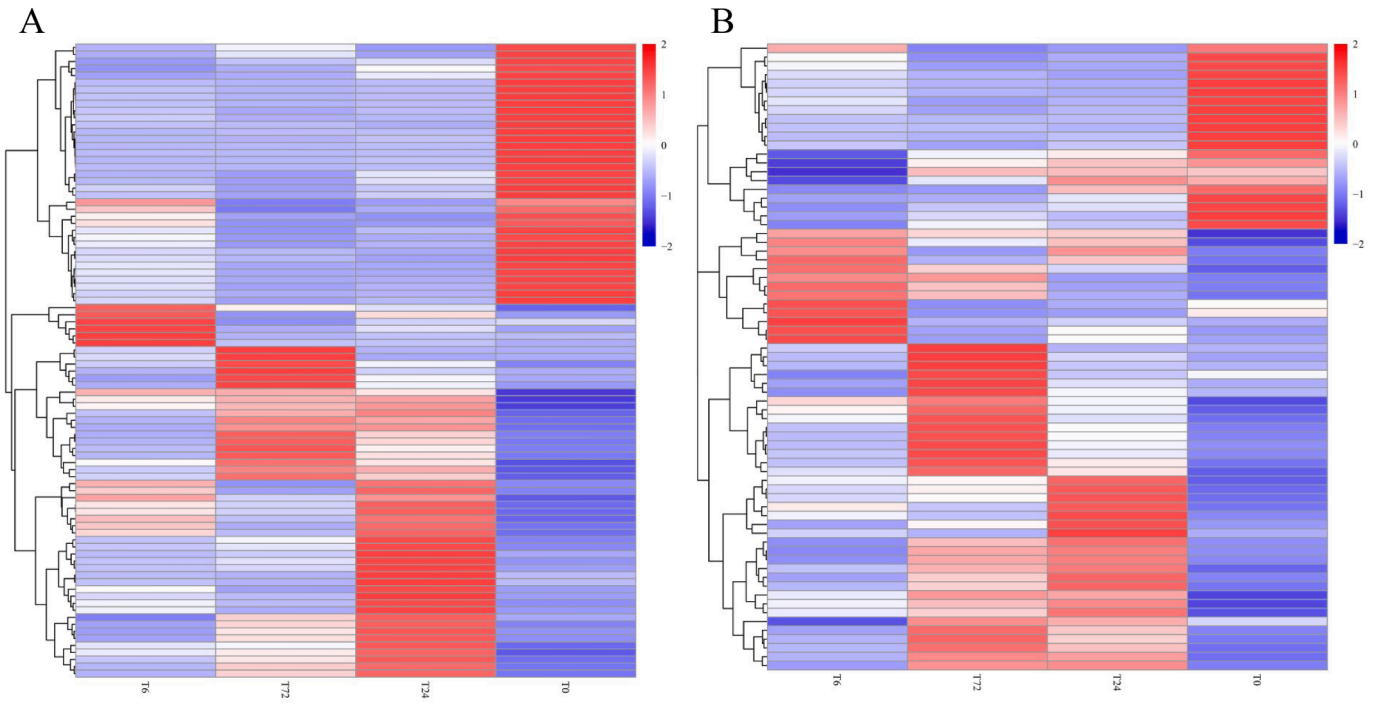

Fig. 4. Hierarchical clustering analysis of differential metabolites of BY6. The vertical direction represents the clustering of the samples, and the horizontal represents the clustering of the metabolites. The length of the clustering branches is inversely proportional to the similarity. The expression patterns of metabolite content among samples can be effectively observed by longitudinal clustering.

the cellular component category was "Membrane" (426 up-regulated and 846 down-regulated DEGs). In the Molecular function category, They were "anion transmembrane transporter activity" (44 up-regulated and 61 down-regulated DEGs) followed by organic anion transmembrane transporter activity molecular function (34 up-regulated and 50 down-regulated DEGs).

3.4. Metabolic analysis and key metabolite identification

As indicated by comparative metabolite results, BY6 bacterial intracellular metabolites were assayed. The results of mass spectrometry detection in positive ion mode, PCA and OPLS-DA score maps show that the spatial separation of metabolites between T0 group and T6, T24 and T72 groups is clear with a good correlation between the biological replicates, QC The samples are centered and clustered tightly, indicating good data quality and overall method stability (Fig. 3). The cluster heatmap directly showed significant differences in intracellular differential metabolite abundances between groups (Fig. 4). Similar results were also seen in the negative ion mode.

After comparing retention time, *m/z* (mass-to-charge ratio), and molecular formula predictions with the mz Cloud database, 496 metabolites were identified (294 from positive ion mode and 202 from negative ion mode). The volcano plot results show that comparing the T0 vs T6 groups of metabolites (Table 1) in the positive ion mode, there are a total of 55 metabolites with significant differences (34 up-regulated, 21 down-regulated). In the negative ion mode, there are a total of 46 metabolites significantly different metabolites (31 up-regulated and 15 down-regulated). Comparing the T0 vs T24 groups of metabolites, there were 65 significantly different metabolites in positive ion mode (41 up-regulated, 24 down-regulated) and 46 significantly different metabolites in negative ion mode (35 up-regulated and 11 down-regulated). Comparing the T0 vs T72 groups of metabolites, there were 50 significantly different metabolites in positive ion mode (36 and 14 down-regulated), and 67 significantly different metabolites in negative ion mode (37 up-regulated, 30 down-regulated).

Table 1
Differential expression metabolite.

Ion mode	Group	Total	up-regulated	Down-regulated
Positive	0 h vs 6 h	55	34	21
	0 h vs 24 h	65	41	24
	0 h vs 72 h	50	36	14
Negative	0 h vs 6 h	46	31	15
	0 h vs 24 h	46	35	11
	0 h vs 72 h	67	37	30

The numbers indicate that BY6 up-regulated more than 1.5 times the differential metabolites after *A. solidipes* induction. The numbers indicates that the differential metabolites are down-regulated by more than 1.5 times after BY6 induction.

3.5. Identification of altered pathways with metabolomic and transcriptomic pathway-based integration

We performed KEGG enrichment analysis to categorize DEGs and DEMS into different pathways based on KEGG database. Scatter plots show the top 20 pathways with the lowest Q value among significantly enriched pathways. Comparing the T0 vs T6 groups of association KEGG pathways enriched results in the identification of the pathways, "Galactose metabolism", "Purine metabolism" and "Biosynthesis of antibiotics" in positive ion mode. "C5-Branched dibasic acid metabolism", "Vancomycin resistance" and "Peptidoglycan biosynthesis" in negative ion mode (Fig. 5 **A1)**. Comparing T0 vs T24 for groups of association in KEGG pathways enrichment identified the pathway, "Glycolysis/ Gluconeogenesis", PTS, and "Vitamin B6 metabolism" in positive ion mode (Fig. 5 **A2)**. In the negative ion mode enriched pathways identified were "Valine, leucine and isoleucine biosynthesis", "Glycolysis/ Gluconeogenesis" and "C5-Branched dibasic acid metabolism". Comparing the T0 vs T72 groups of association KEGG pathways enrichment identified, "Purine metabolism", "Biosynthesis of antibiotics" and "PTS" in positive ion mode (Fig. 5 **A3)**. "Ubiquinone and other terpenoid-quinone biosynthesis", "Galactose metabolism" and "Folate biosynthesis" in

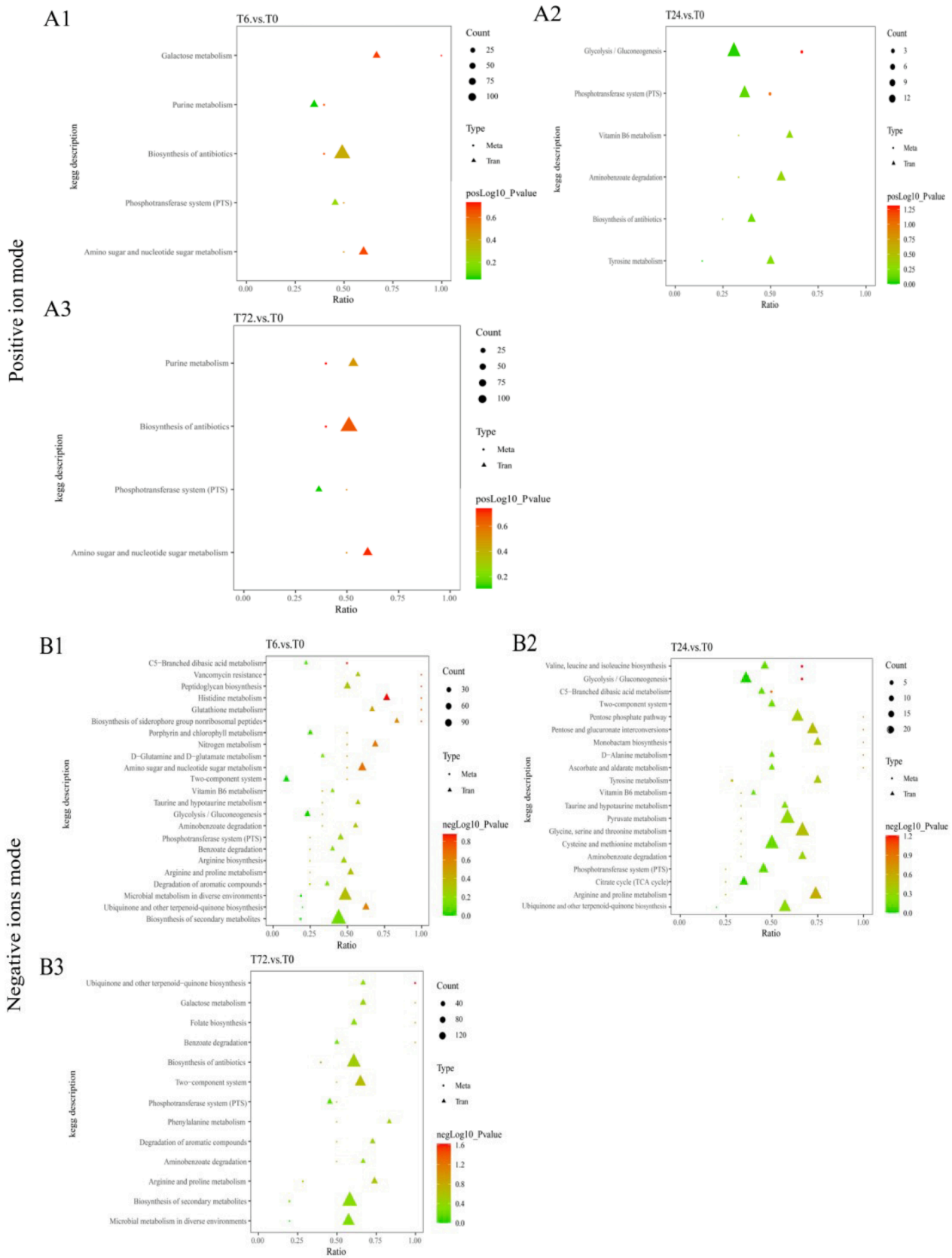

Fig. 5. Integrated interaction analysis of DEGs and DMs annotated pathways. "*P*-value" is the ratio of the enrichment of DEGs or DMs pathways; "Count" is the number of DEGs or DMs enriched in the pathway, The "ratio" is the number of backgrounds. The green to red represents that the ratio increases gradually. (For interpretation of the references to colour in this figure legend, the reader is referred to the web version of this article.)

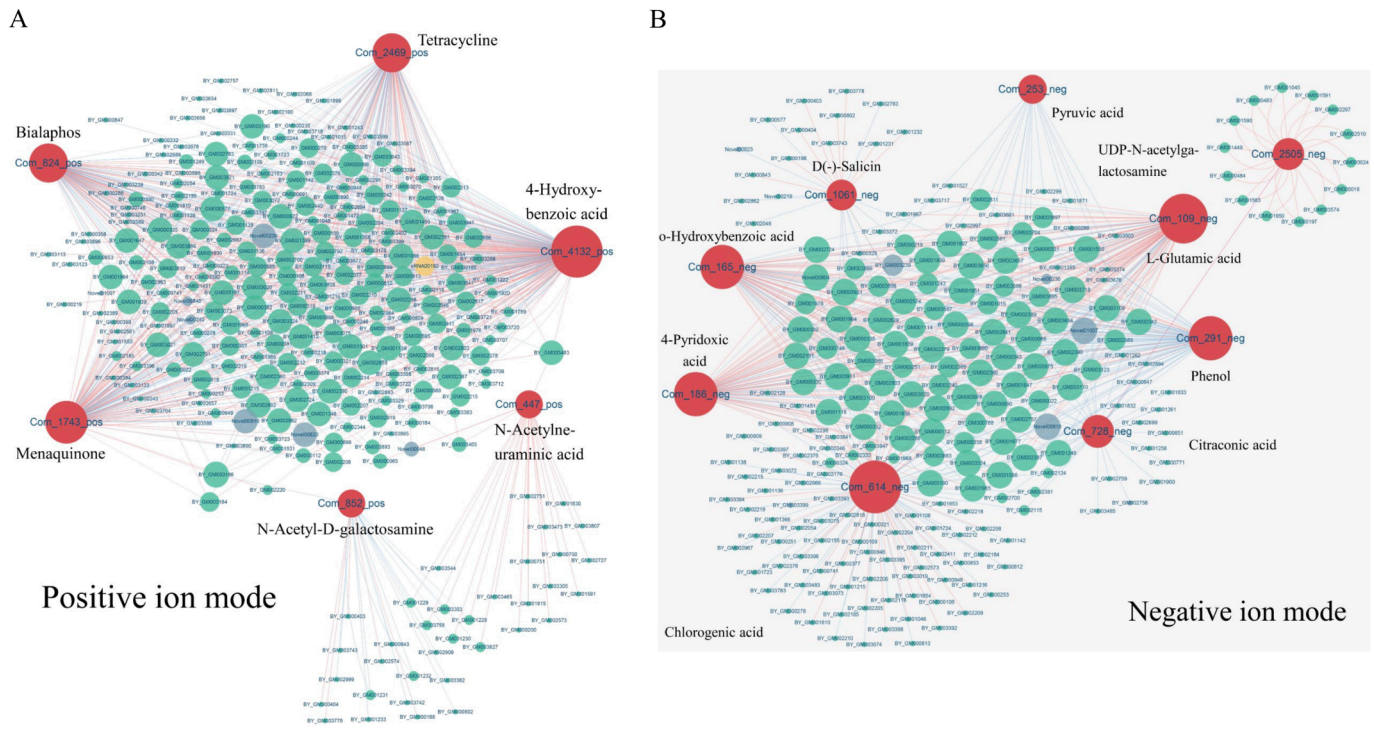

Fig. 6. Analysis of the integrated interaction network of DEGs and DMs pathways. The red connecting line indicates the forward regulation, and the blue connecting line indicates the reverse regulation. Different colors of nodes represent genes (Green), Novel genes (Light blue), sRNA genes (Yellow), and metabolites (Red). The size of each section represents the expression level of related genes or metabolites. (For interpretation of the references to colour in this figure legend, the reader is referred to the web version of this article.)

negative ion mode **(**Fig. 5 **B1 ~ B3)**. Among them, "PTS" had the highest frequency among all groups, followed by "Biosynthesis of antibiotics" and "Ubiquinone and other terpenoid-quinone biosynthesis". Subsequently, we continued to correlate the metabolites and genes expression and link these to the damage observed and growth inhibition of BY6.

3.6. Integrated comprehensive networks analysis of transcriptome and metabolomics

Datasets of statistically significant affected genes and metabolites were evaluated using existing biological knowledge on the metabolic pathways defined by the KEGG database. Discovered by integrative analysis, based on transcriptomic and HPLC-MS metabolomic data, we constructed co-expression networks between metabolites and genes **(Table S4)**. In the positive ion mode **(**Fig. 6**A)**, a total of 6 metabolites were screened, the metabolites Menaquinone and 4-Hydroxy benzoic acid were simultaneously enriched in "Biosynthesis of secondary metabolites" and "Ubiquinone and other terpenoid-quinone biosynthesis" regulatory pathway, The metabolites "N-Acetylne-uraminic acid" and "N-Acetyl-D-galactosamine" are enriched to the "Amino sugar and nucleotide sugar metabolism" and "PTS" pathway, respectively. The metabolites Bialaphos and Tetracycline were enriched in the "Biosynthesis of antibiotics" pathway. The most expressed compound was "4-Hydroxy benzoic acid", followed by Menaquinone.

In negative ion mode **(**Fig. 6**B)**, a total of 9 metabolites, L-Glutamic acid, Phenol, o-Hydroxybenzoic acid (also known as Salicylic acid), 4-Pyridoxic acid and Pyruvic acid, were simultaneously enriched in the "Microbial metabolism in diverse environments" "PTS" and "two-component system" pathway. The most expressed compound was Chlorogenic acid, followed was L-Glutamic acid.

3.7. qRT-PCR validation and expression analysis results

To confirm the RNA-seq results, 24 DEGs that have different roles in "PTS", "Two-component system" and "Ubiquinone and other terpenoid-quinone biosynthesis" were selected. A significant correlation was observed between the RT-qPCR and RNA-seq results **(**Fig. 7**)**, validating the analysis as performed by RNA-seq.

4. Discussion

Bacillus spp. include endophytic bacteria with a broad antimicrobial spectrum and are regarded as an ecofriendly alternative to chemical control of pathogens and pest (Xie et al., 2020). Previously, we have shown that the endophytic BY6 is an efficient biocontrol strain with multiple modes of action, including direct inhibition of growth of pathogens as well as enhancement of immune responses by inducing host system resistance (Zhang et al., 2021). BY6 was isolated from the xylem of an ancient poplar tree, the xylem is in a relatively closed environment and is not easily affected by external environmental factors (Zhang et al., 2021). Some specific endophytes that grow on the xylem can be used as biocontrol agents to directly inhibit pathogenic fungi through the production of antibiotics, spatial competition, or by inducing the plant immune system (Rubini et al., 2005; Jin et al., 2013). In addition, most endophytes isolation studies have focused on from tree leaves (Arnold et al., 2007; Unterseher et al., 2013), and few studies have isolated endophytes from tree xylem (Anguita-Maeso et al., 2021; Anguita-Maeso et al., 2022).

BY6 maintains the shape of cell membranes and cell walls by increasing their mechanical resistance. In this study, it was found that the concentration of BY6 spores (*OD600*) and eDNA first increased and then decreased under in vitro conditions, indicating that *A. solidipes* inhibited the production of BY6 spores and eDNA in the later stage. The intracellular EPS was stable after a rapid increase indicating that the production of intracellular EPS in BY6 was negatively affected. This was corroborated by SEM were we identified that the BY6 cells showed significant changes in morphology. Cells co-cultured with *A. solidipes* were severely deformed, twisted and scattered, with many wrinkles,

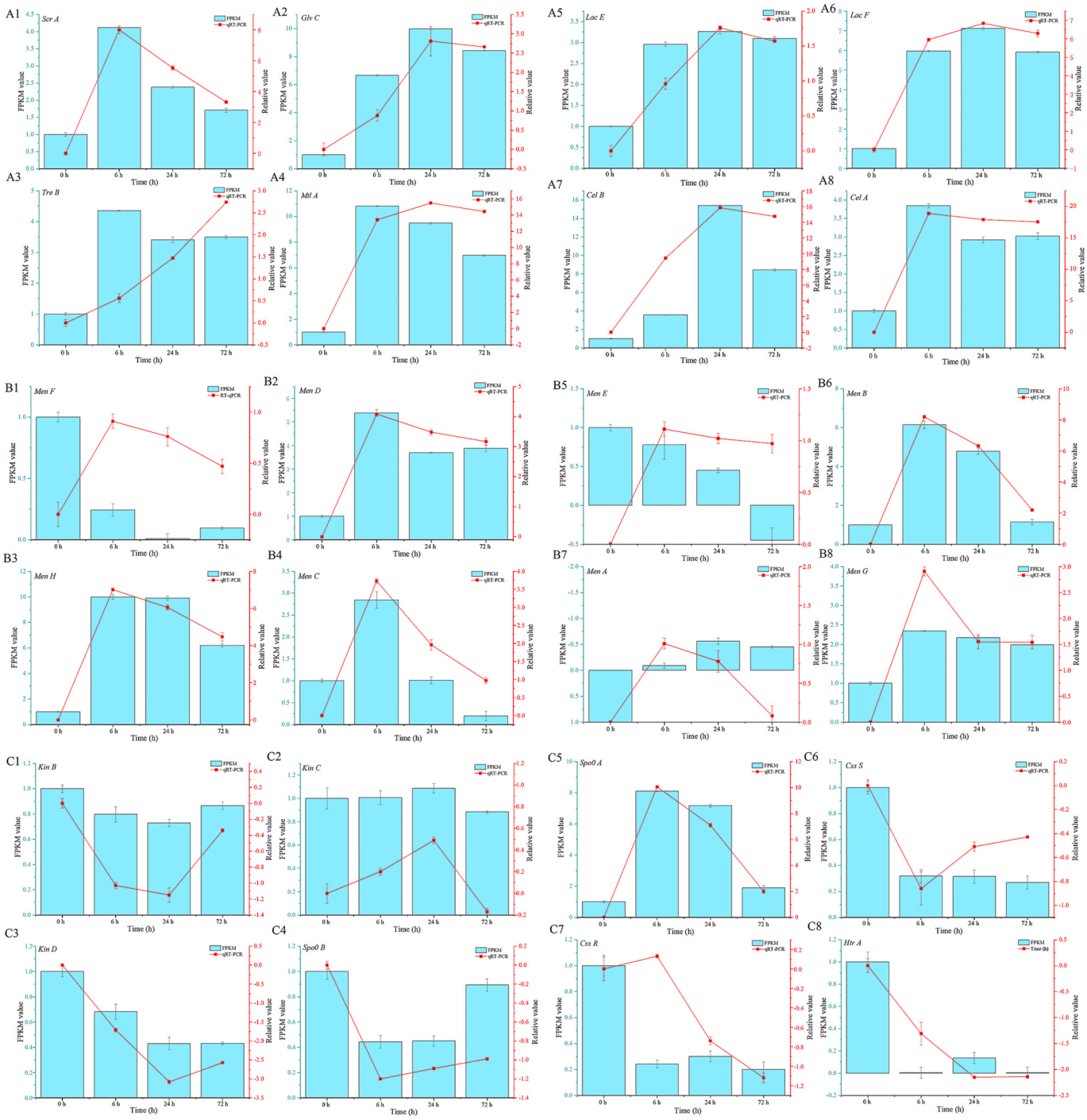

Fig. 7. Gene expression of differentially expressed genes by qRT- PCR. The graph value is the average of 3 biological replicates; the error bars represent the standard error of the average (n = 3) at each time point; 3 replicates. A1 ~ A8 are genes related to "PTS" (Glc family, Fru family, Lac family, Pyruvic acid), representing, *Scr A*, *Glv C*, *Tre B*, *Mtl A*, *Lac E*, *Lac F*, *Cel B* and *Cel A*, respectively. B1 ~ B8 are genes related to "Ubiquinone and other terpenoid-quinone biosynthesis" (Isochorismate, 2-Succinylbenzoate, Menaquinone), representing *Men F*, *Men D*, *Men H*, *Men C*, *Men E*, *Men B*, *Men A* and *Men G*, respectively. C1 ~ C8 are genes related to "Two-component system" (Pyruvic acid), representing, *Kin B*, *Kin C*, *Kin D*, *Spo0 B* and *Spo0 A*, respectively. Full names of the genes are given in Table S 1.

dents and breaks in the cell wall. Similar results were found in some other studies, SEM results showed that *Lactobacillus pentosus* had a strong inhibitory effect on *Bacillus cereus* by destroying the cell wall and cell membrane, cells wrinkling, deforming and twisting mainly in *B. cereus* (Xu et al., 2022). In our previous pot research results, we found that *Bacillus amyloliquefaciens* AW3 showed the same phenomenon in the middle and late stages of controlling Poplar root rot, The AW3 cells attached to the root surface deformed, dissolved and disappeared, hampering AW3 in the middle and late stages of disease control. Upon co-cultivation *A. solidipes* has a strong negative effect on BY6. The cell wall and possibly the cell membrane, likely leading to the leakage of nutrients in BY6 cells. BY6 was unable to maintain its normal growth, showed reduced reproductive ability, and a decreased antifungal activity. This is likely to result in loss of efficacy of BY6 as a biocontrol agent as was found previously for AW3 (Zhang et al., 2022a,b).

To gain molecular insight in the damage caused and the response of BY6 to counteract and regain growth potential we exploited transcriptomics and metabolomics to further analyze the effect of *A. solidipes*

on the growth and inhibition of BY6 cells. Based on the GO enrichment analysis results, the biological process category, "Localization" was the most common term, followed by "Establishment of lacalization" and "Transport". In the cellular components category, the most abundant term was "Membrane", followed by "Cell projection". In the category of molecular functions, the most abundant term was "Transferase activity". Therefore, "Localization", "Transferase activity" and "Membrane" were considered as potential targets of *A. solidipes* to inhibit the growth of BY6 cells. This study indicates that the damage caused by *A. solidipes* is counteracted by altering gene expression and metabolites of the "Membrane" pathway of BY6, decreasing the permeability of the cell membrane, thereby hindering the nutrient uptake, and uptake of toxic substances by BY6 as the membrane system is an important barrier (Dettman et al., 2015; Fira et al., 2018). There are also some studies that Glucose (Glu) can inhibit bacterial cell membrane deformation and damage, significantly enhance the activities of endogenous superoxide dismutase and glutathione peroxidase, and improve the total antioxidant capacity of bacteria. Metabolomics results showed that the content of BY6 intracellular metabolite Pyruvic acid decreased, which could indicate a decreased energy status and would further affect the process of Glu oxidation to form Acetyl-CoA, and the complete oxidation process to water, carbon dioxide and energy through the tricarboxylic acid cycle. This study indicates that *A. solidipes* inhibits BY6 nutrient utilization and oxidative stress, and accelerate the destruction of cell walls and cell membranes, ultimately reducing the ability to control pathogens. In addition, there are several studies showing that both oxidative and secondary oxidative stress in cells are activated when *Bacillus* is exposed to adverse conditions (Mols and Abee, 2011), oxidative stress can strongly activate pro-apoptotic signals, causing programmed cell death (Lee et al., 2019). This study showed that the number of dead cells of BY6 increased, which affected BY6 ability to resist the attack of *A. solidipes*, eventually leading to a decrease in the bacteriostatic ability.

To further reveal the regulatory roles of DEGs, the post-integrated metabolomic and transcriptomic data DEGs were classified to reveal the enrichment of important DEGs by KEGG database pathways. We found that a total of 5397 DEGs were enriched in 305 KEGG pathways, and we screened the top 20 important KEGG pathways. In the positive ion mode, most were mainly enriched in "PTS", "Amino sugar and nucleotide sugar metabolism", and "Aminobenzoate degradation". In the negative ion mode, most were significantly enriched in the following pathways: "Ubiquinone and other terpenoid-quinone biosynthesis", "PTS", "Two-component system" and "Biosynthesis of secondary metabolites" etc. This indicated that changed many important signaling pathways of BY6 were after the induction of *A. solidipes*. Among them, the phosphotransferase system (PTS) pathway has the highest frequency, It is the master regulator of bacterial carbohydrate uptake and is primarily involved in sugar reception, transport and phosphorylation (Reizer et al., 1999; Kang et al., 2021). Meanwhile, in response to carbohydrate availability, "PTS" is involved in regulating functions that are very important in controlling cellular physiological processes, such as biofilm formation, nutrient regulation, motility, and colonization (Barabote and Saier, 2005; Deutscher et al., 2006). Interestingly, in our results, it was found that the genes of the enzyme II complex "Glucose-fructose-lactose Superfamily" in this pathway were all up-regulated, indicating that the resistance of the pathogen *A. solidipes* accelerated the excessive consumption of sugar by BY6. At the same time, the content of pyruvate metabolites in this pathway decreased, we hypothesize that the phosphorylation of "PTS" protein was blocked, and the unphosphorylated EIIAGlc protein inhibited lactose, maltose, transport and phosphorylation of carbon sources such as glycerol. If BY6 cannot transport other carbon sources into the cell it will be deprived of such nutrients which would result in reduced growth and hamper development.

Currently, there is little reported information on the synthetic pathway of BY6 "Ubiquinone and other terpenoid-quinone biosynthesis". Through transcriptome and metabolome correlation results, We found that the metabolite Isochorismate (*Men F*) encoded in the synthetic pathway of "Ubiquinone and other terpenoid-quinone biosynthesis", 2-Succinyl-5-enolpyruvyl-6-hydroxy-3-cyclohexene-1-carboxylate (*Men D*), (1R,6R)-2-Succinyl-6-hydroxy-2,4-cyclohexadiene-1-carboxylate) (*Men H*), 2-Succinylbenzoate (*Men C*), 2-Succinylbenzoyl-CoA (*Men E*), 1,4-Dihydroxy-2-naphthoyl-CoA (*Men B*), 2-Demethyl-menaquinone-8 (*Men A*) down-regulation of genes, The final metabolite menadione (*Men G*) exhibited the same trend. This indicated that the negative regulation of the above genes inhibited the production of the metabolite menadione. Menadione acts as an enzyme cofactor that activates osteocalcin (OC) and matrix Gla protein (MGP), which are involved in important cellular physiology and growth regulation (Hansen et al., 2013). Some studies have pointed out that when the amount of this substance is insufficient in human, animal or bacterial synthesis, it needs to be supplemented by external nutrition (Mandinia et al., 2017). During the culture process of BY6 and *A. solidipes*, we added glucose at four timepoints. However, we found that there was no improvement in the growth of BY6. We speculate that after the phosphorylation of the "PTS" pathway is blocked, carbohydrates cannot enter BY6 cells. Further affects menadione biosynthesis in "Ubiquinone and other terpenoid-quinone biosynthesis" pathways. Therefore, this study provides evidence that the reason for the decline of menadione metabolites may be related to down-regulated genes in the BY6 metabolic pathway. In addition, BY6 is a Gram-positive bacterium that forms dormant sporophytes (Luo et al., 2021). The rate of spore formation is related to the supply of menaquinone. In contrast to the structure of vegetative cells, spore formation is a complex process that may indirectly affect menaquinone production (Delbruck et al., 2022). Although the main steps of the "Ubiquinone and other terpenoid-quinone biosynthesis" pathway have been elucidated, the regulatory mechanism of this pathway still needs to be further explored.

Nutrient deprivation or other unfavorable environmental conditions often prompt *Bacillus* spp. to form endospores for survival (Cano and Borucki, 1995). The transition from vegetative growth to endospore formation represents a major shift in the survival of unicellular bacteria in harsh environments (Hall-Stoodley et al., 2004). Phosphorylation of the *Spo0 A* gene is thought to be critical in this process by activating the multicomponent phosphor layer system. On the one hand, *Spo0 A* directly activates five histidine kinases (*Kin A* ~ *E*) through phosphorylation (Boguslawski et al., 2015); on the other hand, *Spo0 A* is indirectly regulated by *Spo0 F* and *Spo0 B* proteins with phosphate transfer functions (Liu et al., 2022). *Spo0 A* not only regulates spore formation, but also plays an important role in the biofilm formation. A biofilm is seen as a community of bacteria attached to its surface, encased in a self-produced biopolymer matrix, providing a protective place for bacteria (Redman et al., 2020). Compared with cells without biofilm, bacteria encapsulated in biofilm have a stronger inhibitory effect on fungi, and the transcription of biofilm genes is directly regulated by *Spo0 A* ~ *Spo0 B* (Chun et al., 2019; Xu et al., 2019). In this study, BY6 spore and biofilm formation-related genes (*Kin B* ~ *D*) were down-regulated after *A. solidipes* treatment, and the expression levels of *Spo0 A* and *Spo0 B* genes that regulate biofilm were also down-regulated. This study demonstrates that *A. solidipes* leads to the destruction of *BY6* spores and biofilm formation. This disruption promoted BY6 to generate a protective stress response, confirmed by SEM results showing that BY6 cells shrank. Coupled with the restriction of intracellular nutrient utilization of BY6, the results of exopolysaccharide showed that it did not change after the initial increase, which eventually inhibited death. Some studies also show that *Bacillus pentosus* SLC13 accelerates biofilm formation by inhibiting the formation of EPS matrix (Huang et al., 2018). This result indicates that biofilm formation is a more complex physiological process involving more regulatory factors that need to be explored.

In conclusion, this work demonstrates that even though BY6 is able to reduce the growth of *A. solidipes*, reciprocally, *A. solidipes* has a negative effect on BY6 (Zhang et al., 2022b). Upon direct interaction *A. solidipes* causes disrupting BY6 cell membrane integrity, limiting

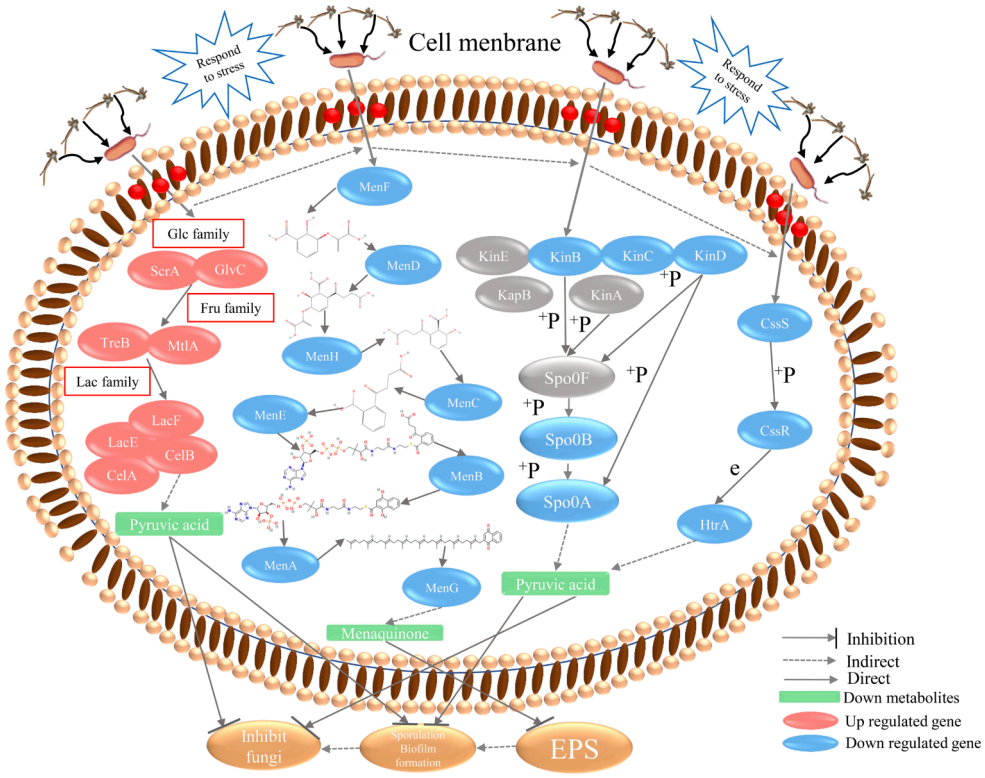

Fig. 8. General overview of the major responsive coercion mechanism of the BY6. Full names of the genes are given in Table S 1.

nutrient utilization, and inhibiting spore and biofilm formation. In this regard, we constructed a responsive coercion mechanism by which BY6 mainly responds to the stress caused by *A. solidipes* (Fig. 8). Overexpression of PTS signaling pathway-related genes (*Scr A*, *Glv C*, *Tre B*, *Mtl A*, *Lac E*, *Lac F*, *Cel A*, *Cel B*) inhibited the expression of metabolite Pyruvic acid, further affecting the expression of "Ubiquinone and other terpenoid-quinone biosynthesis" pathway genes (*Men F*, *Men D*, *Men H*, *Men C*, *Men E*, *Men B*, *Men A*, *Men G*) genes, consequently, the expression of menadione metabolites is inhibited, which is likely to hamper the acquisition of nutrients in BY6 cells. Down-regulation of genes in the "Two-component system" pathway (*Css S, Css R, Htr A, Kin B*, *Kin C*, *Kin D*, *Spo0 B* and *Spo0 A*) is linked to the observed inhibition of BY6 spore and biofilm formation. *A. solidipes* appears to be able to switch the balance between the major metabolic pathways of BY6 nutrient utilization, disrupts the cell wall and membranes, biofilms and spore formation, this could potentially result in the loss of BY6 biocontrol efficacy. In future studies, negative effects of the pathogen towards the biocontrol strain should be taken into account and the observed stress response pathways could be molecular indicators for potential interference of the biological control ability.

CRediT authorship contribution statement

Ping Zhang: Investigation, Methodology, Funding acquisition, Conceptualization, Writing - original draft. **Hao Xin:** Formal analysis, Investigation, Funding acquisition, Software, Visualization. **Theo van der Lee:** Project administration, Supervision, Writing - review & editing.

Declaration of Competing Interest

The authors declare that they have no known competing financial interests or personal relationships that could have appeared to influence the work reported in this paper.

Data availability statement

BY6 complete genome information has been stored in DDBJ/ENA/GenBank, the accession number CP051011-CP051012. Transcriptome raw date stored in NCBI, the BioProject number is PRJNA890047, (https://dataview.ncbi.nlm.nih.gov/object/PRJNA890047?reviewer=7vk4v2s57oiqfp8jbifi07lvfc).

Acknowledgments

This work was supported by supported by "the Fundamental Research Funds for the Central Universities (2572021AW25)" and the Scholarship Council (202006600025). We also would like to thank the reviewers as their suggestions allowed us to improve our manuscript.

Ethical statements

All authors have read and approved the final manuscript. This manuscript is not under consideration by another journal and has not been previously published. This article does not contain any studies with animals performed by any of the authors.

Appendix A. Supplementary data

Supplementary data to this article can be found online at https://doi.org/10.1016/j.biocontrol.2023.105176.

References

Alotaibi, F., St-Arnaud, M., Hijri, M., 2022. In-depth characterization of plant growth promotion potentials of selected alkanes-degrading plant growth-promoting bacterial isolates. Front. Microbiol. 13 https://doi.org/10.3389/fmicb.2022.863702.

Anguita-Maeso, M., Ares-Yebra, A., Haro, C., Roman-ecija, M., Olivares-Garcia, C., Costa, J., Marco-Noales, E., Ferrer, A., Navas-Cortes, J.A., Landa, B.B., 2022. Xylella fastidiosa infection reshapes microbial composition and network associations in the xylem of Almond trees. Front. Microbiol. 13 https://doi.org/10.3389/fmicb.2022.866085.

Anguita-Maeso, M., Trapero-Casas, J.L., Olivares-Garcia, C., Ruano-Rosa, D., Palomo-Rios, E., Jimenez-Diaz, R.M., Navas-Cortes, J.A., Landa, B.B., 2021. *Verticillium dahliae* inoculation and in vitro propagation modify the xylem microbiome and disease reaction to *Verticillium* wilt in a wild Olive genotype. Front. Plant. Sci. 12 https://doi.org/10.3389/fpls.2021.632689.

Arnold, A.E., Henk, D.A., Eells, R.L., Lutzoni, F., Vilgalys, R., 2007. Diversity and phylogenetic affinities of foliar fungal endophytes in loblolly pine inferred by culturing and environmental PCR. Mycologia 99, 185–206. https://doi.org/10.3852/mycologia.99.2.185.

Anders, S., Huber, W., 2012. Differential expression of RNA-Seq data at the gene level-the DESeq package. Heidelberg, Germany: European Molecular Biology Laboratory (EMBL), 10, f1000research. (https://www.genomatix.de/online_help/help_regionminer/DESeq_1.10.1.pdf).

Barabote, R.D., Saier, M.H., 2005. Comparative genomic analyses of the bacterial phosphotransferase system. Microbiol. Mol. Biol. R. 69, 608-+. https://doi.org/10.1128/MMBR.69.4.608-634.2005.

Bertini, I., Hu, X.Y., Luchinat, C., 2014. Global metabolomics characterization of bacteria: pre-analytical treatments and profiling. Metabolomics 10, 241–249. https://doi.org/10.1007/s11306-013-0571-4.

Boguslawski, K.M., Hill, P.A., Griffith, K.L., 2015. Novel mechanisms of controlling the activities of the transcription factors *Spo0A* and coma by the plasmid-encoded quorum sensing regulators Rap60-Phr60 in *Bacillus subtilis*. Mol. Microbiol. 96, 325–348. https://doi.org/10.1111/mmi.12939.

Cano, R.J., Borucki, M.K., 1995. Revival and identification of bacterial-spores in 25-million-year-old to 40-million-year-old *Dominican amber*. Science 268, 1060–1064. https://doi.org/10.1126/science.7538699.

Casamali, B., Chavez, D.J., 2017. Potential of new prunus rootstocks for managing *Armillaria* root rot disease in peach production. J. Am. Pomol. Soc. 71, 82–90.

Chun, B.H., Kim, K.H., Jeong, S.E., Jeon, C.O., 2019. Genomic and metabolic features of the *Bacillus amyloliquefaciens* group-*B. amyloliquefaciens*, *B. velezensis*, and *B. siamensis*- revealed by pan-genome analysis. Food. Microbiol. 77, 146–157. https://doi.org/10.1016/j.fm.2018.09.001.

Delbruck, A.I., Tritten, Y., Nanni, P., Heydenreich, R., Mathys, A., 2022. Moderate high-pressure superdormancy in *Bacillus* spores: properties of superdormant spores and proteins potentially influencing moderate high-pressure germination. Appl. Environ. Microb. 88 https://doi.org/10.1128/aem.02406-21.

Dettman, J.R., Rodrigue, N., Kassen, R., 2015. Genome-wide patterns of recombination in the opportunistic human pathogen *Pseudomonas aeruginosa*. Genome. Bbiol. Evol. 7, 18–34. https://doi.org/10.1093/gbe/evu260.

Deutscher, J., Francke, C., Postma, P.W., 2006. How phosphotransferase system-related protein phosphorylation regulates carbohydrate metabolism in bacteria. Microbiol. Mol. Biol. R. 70, 939-+. https://doi.org/10.1128/MMBR.00024-06.

Dimopoulou, A., Theologidis, I., Benaki, D., Koukounia, M., Zervakou, A., Tzima, A., Diallinas, G., Hatzinikolaou, D.G., Skandalis, N., 2021. Direct antibiotic activity of bacillibactin broadens the biocontrol range of *Bacillus amyloliquefaciens* MBI600. Msphere 6. https://doi.org/10.1128/mSphere.00376-21.

Eljounaidi, K., Lee, S.K., Bae, H., 2016. Bacterial endophytes as potential biocontrol agents of vascular wilt diseases - review and future prospects. Biol. Control. 103, 62–68. https://doi.org/10.1016/j.biocontrol.2016.07.013.

Fira, D., Dimkic, I., Beric, T., Lozo, J., Stankovic, S., 2018. Biological control of plant pathogens by *Bacillus* species. J. Biotechnol. 285, 44–55. https://doi.org/10.1016/j.jbiotec.2018.07.044.

Ghendov-Mosanu, A., Cojocari, D., Balan, G., Patras, A., Lung, I., Soran, M.L., Opris, O., Cristea, E., Sturza, R., 2022. Chemometric optimization of biologically active compounds extraction from grape marc: composition and antimicrobial activity. Molecules 27, 1610. https://doi.org/10.3390/molecules27051610.

Hall-Stoodley, L., Costerton, J.W., Stoodley, P., 2004. Bacterial biofilms: from the natural environment to infectious diseases. Nat. Rev. Microbiol. 2, 95–108. https://doi.org/10.1038/nrmicro821.

Hansen, L., Mathiesen, A.S., Vestergaard, P., Ehlers, L.H., Petersen, K.D., 2013. A health economic analysis of osteoporotic fractures: who carries the burden? Arch. Osteoporos. 8 https://doi.org/10.1007/s11657-013-0126-3.

Huang, M.L., Huang, J.Y., Kao, C.Y., Fang, T.J., 2018. Complete genome sequence of *Lactobacillus pentosus* SLC13, isolated from mustard pickles, a potential probiotic strain with antimicrobial activity against foodborne pathogenic microorganisms. Gut. Pathog 10. https://doi.org/10.1186/s13099-018-0228-y.

Jautzus, T., van Gestel, J., Kovacs, A.T., 2022. Complex extracellular biology drives surface competition during colony expansion in *Bacillus subtilis*. Isme. J. 16, 2320–2328. https://doi.org/10.1038/s41396-022-01279-8.

Jha, S., Bhadani, N.K., Kumar, A., Sengupta, T.K., 2022. Glucose-induced biofilm formation in *Bacillus thuringiensis* KPWP1 is associated with increased cell surface hydrophobicity and increased production of exopolymeric substances. Curr. Microbiol. 79 https://doi.org/10.1007/s00284-021-02699-z.

Jin, H., Yan, Z.Q., Liu, Q., Yang, X.Y., Chen, J.X., Qin, B., 2013. Diversity and dynamics of fungal endophytes in leaves, stems and roots of *Stellera chamaejasme* L. in northwestern China. Anton. Leeuw. Int. J. G.104, 949–963. https://doi.org/10.1007/s10482-013-0014-2.

Kang, D., Ham, H.I., Lee, S.H., Cho, Y.J., Kim, Y.R., Yoon, C.K., Seok, Y.J., 2021. Functional dissection of the phosphotransferase system provides insight into the prevalence of *Faecalibacterium prausnitzii* in the host intestinal environment. Environ. Microbiol. 23, 4726–4740. https://doi.org/10.1111/1462-2920.15681.

Kedves, O., Shahab, D., Champramary, S., Chen, L.Q., Indic, B., Boka, B., Nagy, V.D., Vagvolgyi, C., Kredics, L., Sipos, G., 2021. Epidemiology, biotic interactions and biological control of *Armillarioids* in the northern hemisphere. Pathogens 10, 76. https://doi.org/10.3390/pathogens10010076.

Kilic, T., Cihan, A.C., 2020. Biofilm formation of the facultative thermophile *Bacillus pumilus* D194A and affects of sanitation agents on its biofilms. Microbiology+ 89, 64–73. https://doi.org/10.1134/S0026261720010087.

Kloepper, J.W., Ryu, C.M., Zhang, S.A., 2004. Induced systemic resistance and promotion of plant growth by *Bacillus spp*. Phytopathology 94, 1259–1266. https://doi.org/10.1094/PHYTO.2004.94.11.1259.

Kulimushi, P.Z., Arias, A.A., Franzil, L., Steels, S., Ongena, M., 2017. Stimulation of fengycin-type antifungal lipopeptides in *Bacillus amyloliquefaciens* in the presence of the maize fungal pathogen *Rhizomucor variabilis*. Front. Microbiol. 8 https://doi.org/10.3389/fmicb.2017.00850.

Langmead, B., Salzberg, S.L., 2012. Fast gapped-read alignment with Bowtie 2. Nat methods. 9, 357–359. https://doi.org/10.1038/nmeth.1923.

Lee, D., Lee, S.H., Noh, I., Oh, E., Ryu, H., Ha, J., Jeong, S., Yoo, J., Jeon, T.J., Yun, C.O., Kim, Y.C., 2019. A helical polypeptide-based potassium ionophore induces endoplasmic reticulum stress-mediated apoptosis by perturbing ion homeostasis. Adv. Sci. 6 https://doi.org/10.1002/advs.201801995.

Liu, N., Chen, B., Zhao, X.Y., Wen, J.H., Qi, G.F., 2022. Cations and surfactin serving as signal molecules trigger quorum sensing in *Bacillus amyloliquefaciens*. J. Basic. Microb. 62, 35–47. https://doi.org/10.1002/jobm.202100315.

Luo, C.P., Liu, J.C., Bilal, M., Liu, X.H., Wang, X.H., Dong, F., Liu, Y., Zang, S.S., Yin, X.L., Yang, X.T., Zhu, T., Zhang, S.Y., Zhang, W.F., Li, B., 2021. Extracellular lipopeptide bacillomycin l regulates serial expression of genes for modulating multicellular behavior in *Bacillus velezensis* Bs916. Appl. Microbiol. Biot. 105, 6853–6870. https://doi.org/10.1007/s00253-021-11524-3.

Mandinia, E., Demirci, A., Berenjian, A., 2017. Production and application of menaquinone-7 (vitamin k2): a new perspective. World. J. Microb. Biot. 33 https://doi.org/10.1007/s11274-016-2169-2.

Mols, M., Abee, T., 2011. Primary and secondary oxidative stress in *Bacillus*. Environ. Microbiol. 13, 1387–1394. https://doi.org/10.1111/j.1462-2920.2011.02433.x.

Ongena, M., Jacques, P., 2008. *Bacillus* lipopeptides: versatile weapons for plant disease biocontrol. Trends. Microbiol. 16, 115–125. https://doi.org/10.1016/j.tim.2007.12.009.

Otasek, D., Morris, J.H., Boucas, J., Pico, A.R., Demchak, B., 2019. Cytoscape automation: empowering workflow-based network analysis. Genome. Biol. 20 https://doi.org/10.1186/s13059-019-1758-4.

Pandin, C., Darsonval, M., Mayeur, C., Le Coq, D., Aymerich, S., Briandet, R., 2019. Biofilm formation and synthesis of antimicrobial compounds by the biocontrol agent *Bacillus velezensis* QST713 in an *Agaricus bisporus* compost micromodel. Appl. Environ. Microb. 85 https://doi.org/10.1128/AEM.00327-19.

Radhakrishnan, R., Hashem, A., Abd Allah, E.F., 2017. *Bacillus*: a biological tool for crop improvement through bio-molecular changes in adverse environments. Front. Physiol. 8 https://doi.org/10.3389/fphys.2017.00667.

Redman, W.K., Welch, G.S., Rumbaugh, K.P., 2020. Differential efficacy of glycoside hydrolases to disperse biofilms. Front. Cell. Infect. Mi. 10 https://doi.org/10.3389/fcimb.2020.00379.

Reizer, J., Bachem, S., Reizer, A., Arnaud, M., Saier, M.H., Stulke, J., 1999. Novel phosphotransferase system genes revealed by genome analysis - the complete complement of PTS proteins encoded within the genome of *Bacillus subtilis*. Microbiology-UK 145, 3419–3429. https://doi.org/10.1099/00221287-145-12-3419.

Rubini, M.R., Silva-Ribeiro, R.T., Pomella, A., Maki, C.S., Araujo, W.L., Dos Santos, D.R., Azevedo, J.L., 2005. Diversity of endophytic fungal community of Cacao (*Theobroma cacao* L.) and biological control of *Crinipellis perniciosa*, causal agent of witches' broom disease. Int. J. Biol. Sci. 1, 24–33. https://doi.org/10.7150/ijbs.1.24.

Saravanakumar, D., Thomas, A., Banwarie, N., 2019. Antagonistic potential of Lipopeptide producing *Bacillus amyloliquefaciens* against major vegetable pathogens. Eur. J. Plant Pathol. 154, 319–335. https://doi.org/10.1007/s10658-018-01658-y.

Stoll, A., Salvatierra-Martinez, R., Gonzalez, M., Araya, M., 2021. The role of Surfactin production by *Bacillus velezensis* on colonization, biofilm formation on tomato root and leaf surfaces and subsequent protection (ISR) against *Botrytis cinerea*. Microorganisms 9, 2251. https://doi.org/10.3390/microorganisms9112251.

Teklu, B.M., Haileslassie, A., Mekuria, W., 2022. Pesticides as water pollutants and level of risks to environment and people: an example from Central Rift Valley of Ethiopia. Environ. Dev. Sustain. 24, 5275–5294. https://doi.org/10.1007/s10668-021-01658-9.

Unterseher, M., Persoh, D., Schnittler, M., 2013. Leaf-inhabiting endophytic fungi of European beech (*Fagus sylvatica* L.) Co-occur in leaf litter but are rare on decaying wood of the same host. Fungal. Divers. 60, 43–54. https://doi.org/10.1007/s13225-013-0222-0.

Vlamakis, H., Chai, Y.R., Beauregard, P., Losick, R., Kolter, R., 2013. Sticking together: building a biofilm the *Bacillus subtilis* way. Nat. Rev. Microbiol. 11, 157–168. https://doi.org/10.1038/nrmicro2960.

Xie, S., Vallet, M., Sun, C., Kunert, M., David, A., Zhang, X.C., Chen, B.H., Lu, X.M., Boland, W., Shao, Y.Q., 2020. Biocontrol potential of a novel endophytic bacterium from Mulberry (*Morus*) tree. Front. Bioeng. Biotech. 7 https://doi.org/10.3389/fbioe.2019.00488.

Xu, Z.H., Mandic-Mulec, I., Zhang, H.H., Liu, Y., Sun, X.L., Feng, H.C., Xun, W.B., Zhang, N., Shen, Q.R., Zhang, R.F., 2019. Antibiotic bacillomycin D affects iron acquisition and biofilm formation in *Bacillus velezensis* through a Btr-mediated feu ABC-dependent pathway. Cell Rep. 29, 1192-+. https://doi.org/10.1016/j.celrep.2019.09.061.

Xu, Z.Q., Yang, Q.L., Zhu, Y.L., 2022. Transcriptome analysis reveals the molecular mechanisms of the novel *Lactobacillus pentosus* pentocin against *Bacillus cereus*. Food. Res. Int. 151 https://doi.org/10.1016/j.foodres.2021.110840.

Yao, J., Allen, C., 2007. The plant pathogen *Ralstonia solanacearum* needs aerotaxis for normal biofilm formation and interactions with its Tomato host. J. Bacteriol. 189, 6415–6424. https://doi.org/10.1128/JB.00398-07.

Zhang, P., Diao, J., Xie, G.Q., Ma, L., Wang, L.H., 2021. A complete genome sequence of the wood stem endophyte *Bacillus velezensis* BY6 strain possessing plant growth-promoting and antifungal activities. Biomed. Res. Int. 2021 https://doi.org/10.1155/2021/3904120.

Zhang, P., Hao, H.T., Wang, L.H., Liu, Z.H., Ma, L., 2022a. Endophytes *Bacillus amyloliquefaciens* AW3 (CGMCC1.16683) improves the growth of *Populus davidiana* x *Populus bolleana* (Pdpap) and induces its resistance to wilt disease by *Fusarium oxysporum* fox68 (CFCC86068). Eur. J. Plant. Pathol. 162, 1–17. https://doi.org/10.1007/s10658-021-02381-x.

Zhu, Y., Xu, Y., Yang, Q., 2021. Antifungal properties and AFB1 detoxification activity of a new strain of *Lactobacillus plantarum*. J. Hazard. Mater. 414, 125569 https://doi.org/10.1016/j.jhazmat.2021.125569.

Zhang, P., Xie, G.Q., Wang, L.H., Xing, Y.Q., 2022b. *Bacillus velezensis* BY6 promotes growth of poplar and improves resistance contributing to the biocontrol of *Armillaria solidipes*. Microorganisms. 10, 2472. https://doi.org/10.3390/microorganisms10122472.

Zhang, B., Sun, B.S., Jin, M., Gong, T.S., Gao, Z.H., 2008. Extraction and analysis of extracellular polymeric substances in membrane fouling in submerged MBR. Desalination 227, 286–294. https://doi.org/10.1016/j.desal.2007.06.032.